Editors' Suggestion

Probing Berry Curvature in Magnetic Topological Insulators through Resonant Infrared Magnetic Circular Dichroism

Seul-Ki Bac,[1,2,9] Florian Le Mardelé,[3] Jiashu Wang,[1] Mykhaylo Ozerov,[4] Kota Yoshimura,[1] Ivan Mohelský,[3] Xingdan Sun,[3] Benjamin A. Piot,[3] Stefan Wimmer,[5] Andreas Ney,[5] Tatyana Orlova,[6] Maksym Zhukovskyi,[6] Günther Bauer,[5] Gunther Springholz,[5] Xinyu Liu,[1] Milan Orlita,[3,7] Kyungwha Park,[8] Yi-Ting Hsu,[1,*] and Badih A. Assaf[1,†]

[1]*Department of Physics and Astronomy, University of Notre Dame, Notre Dame, Indiana 46556, USA*
[2]*KU Leuven, Quantum Solid State Physics, Leuven, Belgium*
[3]*LNCMI-EMFL, CNRS UPR3228, Univ. Grenoble Alpes, Univ. Toulouse, Univ. Toulouse 3, INSA-T, Grenoble and Toulouse, France*
[4]*National High Magnetic Fields Laboratory, Florida State University, Tallahassee, Florida 32310, USA*
[5]*Institut für Halbleiter und Festkörperphysik, Johannes Kepler Universität, 4040 Linz, Austria*
[6]*Notre Dame Integrated Imaging Facility, University of Notre Dame, Notre Dame, Indiana 46556, USA*
[7]*Institute of Physics, Charles University, Ke Karlovu 5, Prague 121 16, Czech Republic*
[8]*Department of Physics, Virginia Tech, Blacksburg, Virginia 24061, USA*
[9]*Institut des NanoSciences de Paris, UPMC, CNRS, 4 place Jussieu, 75005 Paris, France*

(Received 6 June 2024; revised 3 October 2024; accepted 22 November 2024; published 2 January 2025; corrected 5 September 2025)

Probing the quantum geometry and topology in condensed matter systems has relied heavily on static electronic transport experiments in magnetic fields. Yet, contact-free optical measurements have rarely been explored. Here, we report the observation of resonant magnetic circular dichroism (MCD) in the infrared range in thin film $MnBi_2Te_4$ exhibiting a spectral intensity that correlates with the anomalous Hall effect. Both phenomena emerge with a field-driven phase transition from an antiferromagnet to a canted ferromagnet. By theoretically relating the MCD to the anomalous Hall effect via Berry curvature for a metallic state, we show that this transition accompanies an abrupt onset of Berry curvature, signaling a topological phase transition from a topological insulator to a doped Chern insulator. Our density functional theory calculation suggests the MCD signal mainly originates from an optical transition at the Brillouin zone edge, hinting at a potential new source of Berry curvature away from the commonly considered $\mathbf{\Gamma}$ point. Our findings demonstrate a novel experimental approach for detecting Berry curvature through spectroscopy of the interband MCD, generally applicable to magnetic materials.

DOI: 10.1103/PhysRevLett.134.016601

Resonant photoabsorption magnetic circular dichroism (MCD) refers to the optical response of a magnetic material that preferentially absorbs light of a specific circular polarization direction [Figs. 1(b) and 1(c)]. [1] Resonant MCD has been employed to probe the Zeeman splitting and spin polarization of magnetic semiconductors [2–4]. More recently, it was employed to identify a topologically nontrivial phase in ultracold atomic lattices [5–8]. Theoretical efforts in linking optical and photoemission measurements to the quantum mechanical geometry of the Bloch states in emerging magnetic and topological materials have brought new light to the information that MCD carries [9–15].

In particular, resonant absorption MCD in magnetic insulators was recently related to the Chern number [10] responsible for the quantized anomalous Hall effect and arising from Berry curvature (BC), [14,16] the imaginary part of the quantum geometric tensor [13]. Infrared (IR) MCD, resonant with optical transitions involving BC-hosting bands, is, therefore, a novel approach for detecting the band geometry and topology [10]. To date, no experimental measurements of a BC-induced resonant MCD in photoabsorption manifesting a topological phase transition have been reported. Magnetic topological insulators (TIs) characterized by a Chern number are an ideal platform to experimentally detect BC-induced MCD. However, as most topological materials are degenerately doped in the bulk, a relation between MCD and BC is required for the metallic state. Motivated by recent advances in the study of topological properties through optical response [9,12,17–19], this Letter aims to demonstrate how resonant MCD probes the changing topological character of the antiferromagnetic TI $MnBi_2Te_4$ despite its native doping, as a proof of concept that MCD encodes information about the BC.

$MnBi_2Te_4$ [Fig. 1(a)] is a magnetic TI that exhibits a rich phase diagram. It is, hence, an interesting platform to

*Contact author: yhsu2@nd.edu
†Contact author: bassaf@nd.edu

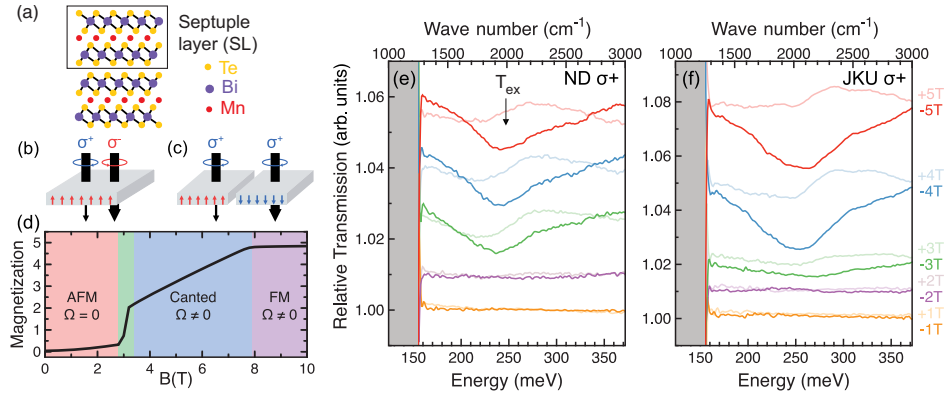

FIG. 1. (a) Crystal structure of $MnBi_2Te_4$ consisting of septuple layers separated by a van der Waals gap. (b) Magnetic circular dichroism (MCD) manifesting as an absorption of light dependent on the direction of circular polarization and (c) as a nonreciprocal absorption of circularly polarized light at opposite magnetic states of a material. (d) Magnetic phase diagram of $MnBi_2Te_4$, Ω is the Berry curvature. AFM, antiferromagnet; FM, ferromagnet. Relative transmission spectra at different magnetic fields at $T = 4.2$ K with a defined polarization for the (e) ND and (f) JKU samples. T_{ex} marks the optical transition studied in this Letter.

search for BC-induced MCD [20–25] In $MnBi_2Te_4$, Mn spins within the Mn layers are coupled ferromagnetically whereas the interlayer coupling is antiferromagnetic. A-type antiferromagnetic $MnBi_2Te_4$ was found to be a TI [26–29]. For thin films and flakes, experiments found a topological phase transition driven by an out-of-plane magnetic field from an antiferromagnetic TI at zero field to a canted ferromagnetic state, and finally to ferromagnetic saturation. [26–28] The latter two phases were suggested to be Chern insulators through the observation of chiral edge states [30–32]. As-grown thin films of $MnBi_2Te_4$ are, however, naturally metallic, making the detection of edge states challenging [26,33]. This motivates alternative probes of the changing topological character of $MnBi_2Te_4$ through its phase diagram. A large IR Faraday and Kerr rotation were recently predicted in ferromagnetic $MnBi_2Te_4$ when time-reversal symmetry is broken [9,19] and a large band-edge BC is activated. This BC generates a nonzero optical Hall conductivity $\sigma_{xy}(\omega)$ and must also yield a resonant MCD that has yet to be observed.

We report the observation of resonant IR-MCD in $MnBi_2Te_4$ films that onsets at the field-driven phase transition into the canted ferromagnetic state. The MCD and the associated optical transition are absent in the antiferromagnetic state. We attribute the manifestation of the MCD to the abrupt onset of BC when $MnBi_2Te_4$ undergoes a topological phase transition from an antiferromagnetic TI to a doped Chern insulator [Fig. 1(c)]. First, the MCD signal is extracted from the measured optical absorption spectroscopy and tied to the magnetization. Second, the first negative moment of the antisymmetric (dissipative) part of the optical Hall conductivity $\sigma_{A,xy}(\omega)$ is theoretically related to the BC even in metallic states, and is shown to be proportional to the nonquantized anomalous Hall conductivity. This relation indicates that the onset of the MCD signal originates from the onset of BC in the canted phase. Third, the intensity of the measured MCD scales with the static anomalous Hall conductivity, confirming its relation to BC. A comparison between the magneto-optical response, the Hall response, and first-principles calculations allows us to infer that this MCD likely originates from an optical transition at the vertical Brillouin zone boundary. Our findings directly detect the onset of BC of Bloch bands along with the bands and momenta responsible for it, which enables the extraction of topological indices [10] and the optical detection of topological phase transitions in future studies.

To unveil the MCD of $MnBi_2Te_4$, we employ magneto-optical IR spectroscopy and measure thin films grown on GaAs(111) (ND) and $SrF_2(111)$ (JKU) by molecular beam epitaxy [34]. With a fixed circular polarization, we detect the MCD as a nonreciprocity in the relative optical transmission when the polarity of the magnetic field B is switched [Fig. 1(b)]. The relative transmission is defined as $\tau = T_S(B)/T_S(0)$, where $T_S(B)$ is the transmission through the sample (B is parallel to the c axis). The MCD is plotted in Figs. 1(e) and 1(f). Below 3 T, the relative transmission is close to 1 and has no energy dependence regardless of the direction of the magnetic field for either sample. At 3 T and above, a minimum marked T_{ex} in Fig. 1(e) is observed only when the magnetic field is negative. The intensity of the MCD is extracted at $|B|$ using

$$\frac{\tau(+B) - \tau(-B)}{\tau(+B) + \tau(-B)} = \mathrm{MCD}(\%).$$

It is plotted as a function of energy in Figs. 2(a) and 2(b) and appears as a peak between 200 and 300 meV. The integrated intensity of the MCD signal is subsequently extracted and plotted in Fig. 2(c). The dichroism emerges at the spin-flop (SF) transition B_{SF} and gains intensity

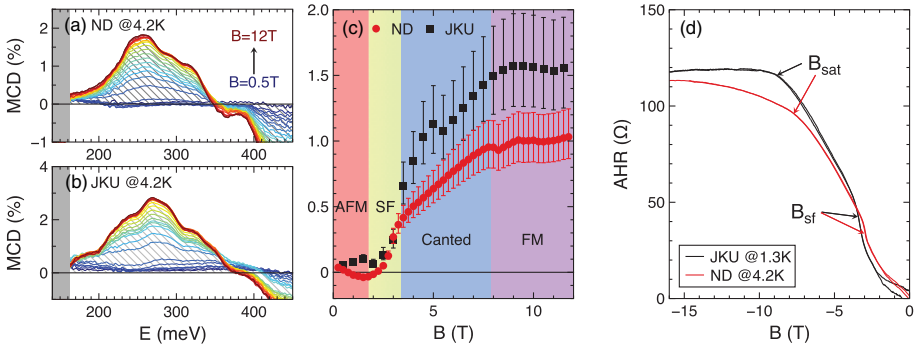

FIG. 2. (a),(b) Magnetic circular dichroism (MCD) in % as a function of energy for different magnetic field strengths for two $MnBi_2Te_4$ samples studied in Fig. 1 (ND and JKU). MCD measurements are taken at $T = 4.2$ K. (c) Integrated MCD versus magnetic field. AFM, antiferromagnetic; SF, spin-flop transition. The integral is done between 200 and 290 meV, the range over which the wave plate induces a phase shift of $\pi/2$ within a 25% tolerance (see [34]). The error bars are obtained by varying this tolerance by ±5%. (d) Anomalous Hall resistance (AHR) measured for the two samples. B_{SF} denotes the spin-flop transition, and B_{sat} denotes the saturation field.

with increasing field. In $MnBi_2Te_4$, 2 T marks the phase boundary of the antiferromagnetic ground state. Above 2 T, a surface SF transition followed by a bulk SF lead to a canted phase. It persists up to saturation to ferromagnetism at B_{sat} [26–28]. The behavior of anomalous Hall effect (AHE), plotted in Fig. 2(d), allows us to extract B_{SF} for both samples. $B_{SF} = 2.95$ T for ND and 3.1T for JKU, consistent with the delayed onset of the MCD observed in the JKU sample. Complete Hall and magnetometry measurements are shown in [34]. Magnetic canting breaks time-reversal symmetry, which induces a topological phase transition to a state with finite Berry curvature above the SF, activating the AHE and the MCD. Both the AHE [Fig. 2(d)] and the MCD signal [Fig. 2(c)] increases in strength as of 2 T, consistent with the activation of BC as $MnBi_2Te_4$ undergoes a transition from from an antiferromagnetic TI to a doped Chern insulator.

We understand the emergence of the MCD in the canted magnetic state through the following symmetry argument. The MCD signal can be expressed as the difference between the absorption of oppositely polarized light $\sigma^+(\omega) - \sigma^-(\omega) = -2\mathrm{Im}(\sigma_{H,xy}(\omega))$, where $\mathrm{Im}(\sigma_{H,xy}(\omega))$ is the imaginary part of the dissipative (Hermitian) optical conductivity. $\mathrm{Im}(\sigma_{H,xy}(\omega))$ is also given by the imaginary part of the antisymmetric optical conductivity $\sigma_{A,xy}(\omega) = \frac{1}{2}(\sigma_{xy}(\omega) - \sigma_{yx}(\omega))$. According to the Onsager relation, the optical conductivity obeys $\sigma_{xy}(\omega, M) = \sigma_{xy}(\omega, -M)$ for opposite magnetization M, and thus becomes symmetric in the Cartesian coordinate system when $M = 0$. It follows that the antisymmetric part vanishes at $M = 0$ such that $\sigma_{A,xy}(\omega, 0) = 0$. Therefore, we expect that the MCD signal vanishes in the antiferromagnetic state, grows with increasing magnetization strength M upon entering the canted state, and saturates to a maximum value in the ferromagnetic state, as was observed in our experiment [Fig. 2(c)].

While the MCD signal directly detects the magnetization strength, its first negative moment is known to be related to the Berry curvature and the static anomalous Hall conductivity $\sigma_{xy}(\omega = 0)$ through the Hall sum rule at temperature T = 0 K [10,14,35] as

$$\mathrm{Im}\left(\int_0^\infty d\omega \frac{\sigma_{A,xy}}{\omega}\right) = -\frac{\pi e^2}{2\hbar}\int \frac{d\boldsymbol{k}}{(2\pi)^3}\sum_n^{occ} f(\hbar\omega_{n,\boldsymbol{k}})\Omega_{xy,n,\boldsymbol{k}} = \frac{\pi}{2}\sigma_{xy}(\omega = 0), \quad (1)$$

where $-e$ is the electron charge and, theoretically, the frequency (energy) cutoff $\omega_c \to \infty$. The key quantity in Eq. (1) is the Berry curvature $\Omega_{xy,n,\boldsymbol{k}}$ of band n,

$$\Omega_{n,\boldsymbol{k},xy} = -2\hbar^2\mathrm{Im}\sum_m^{unocc}\frac{\langle u_{n,\boldsymbol{k}}|v_x|u_{m,\boldsymbol{k}}\rangle\langle u_{m,\boldsymbol{k}}|v_y|u_{n,\boldsymbol{k}}\rangle}{(\omega_{n,\boldsymbol{k}} - \omega_{m,\boldsymbol{k}})^2}$$

where $u_{n,\boldsymbol{k}}$ is the periodic part of the magnetic Bloch wave function, $\omega_{n,\boldsymbol{k}}$ is the energy of band n at wavevector k, and v_i is the velocity operator in the $i = x, y$ direction. Note that since the $MnBi_2Te_4$ samples we investigate are naturally doped, the number of occupied bands n and unoccupied bands m in the summations can be different at different crystal momenta $\boldsymbol{k}$. The right-hand side of the sum rule is proportional to the static anomalous Hall conductivity [36], which we experimentally found to onset in the canted ferromagnetic phase [see Fig. 2(d)]. See [34] for the derivation of this sum rule [10,35,37]. In our experiment, the frequency integration is over the infrared range that covers the low-energy regime in $MnBi_2Te_4$. We therefore expect that the sum rule approximately holds since contributions from bands far away from the Fermi level are suppressed by the frequency appearing in the denominator in the expression for $\Omega_{n,\boldsymbol{k},xy}$. Therefore, our measured MCD signal is directly tied to the BC and the AHE through the sum rule [Eq. (1)] and experimentally through the data in Fig. 2.

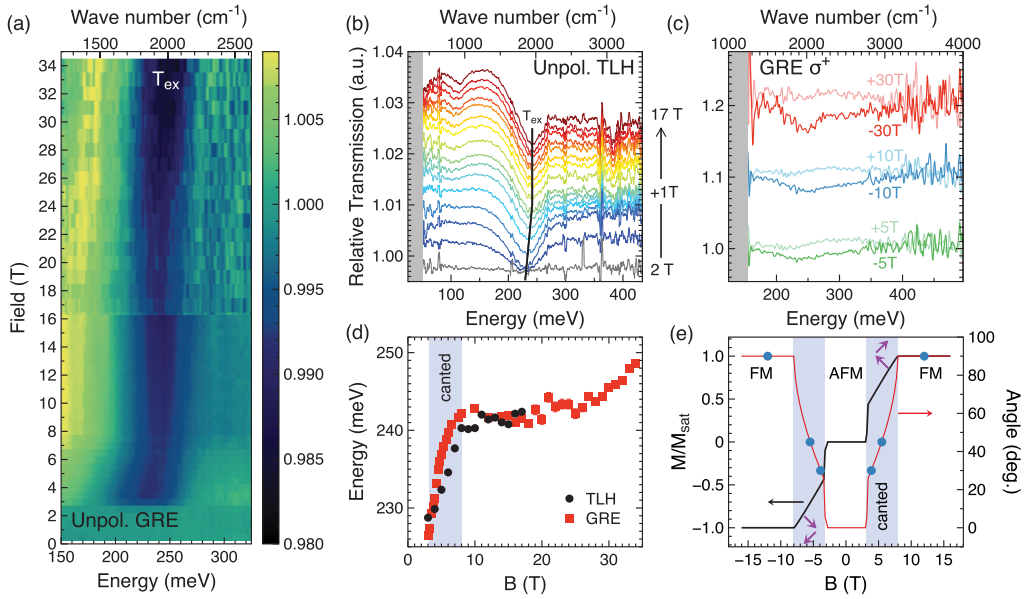

FIG. 3. Unpolarized relative transmission spectra of sample ND at different magnetic fields up to (a) 34 T measured in Grenoble (GRE) and (b) 17 T measured in Tallahassee (TLH). (c) Relative transmission spectra acquired with a defined σ^+ polarization up to 30 T for sample ND. (d) Variation of the energy of T_{ex} as a function of magnetic field. The blue region highlights the canted magnetic phase of $MnBi_2Te_4$. (e) Magnetization relative to saturation (black curve) and canting angle with respect to the basal plane (red curve) of $MnBi_2Te_4$ computed using the Mills' model for a magnetic field applied along the c axis. FM, ferromagnet; AFM, antiferromagnet. The canted phase is illustrated by the purple arrows in (e). The blue circles represent the magnetic states used for the first-principles calculations.

We further show that the energy of the optical transition exhibiting MCD is determined by the intrinsic magnetization of $MnBi_2Te_4$ and not by Zeeman splitting confirming its relation to BC. The relative transmission spectra of the ND sample are presented in Figs. 3(a) and 3(b) for different magnetic fields. The measurements yield the optical transition labeled T_{ex} between 230 and 260 meV. Under circular polarization, T_{ex} exhibits a dichroism up to 30 T [Fig. 3(c)]. We track its field dependence in Fig. 3(d). Its energy increases between 3 and 8 T and then saturates above 8 T, consistent with the magnetization of $MnBi_2Te_4$ computed using the Mills model with parameters constrained by previous measurements [26,27] [Fig. 3(e)]. Above 28 T, the behavior of T_{ex} is not captured by the Mills model, [26,27,38] and is believed to originate from the response of Mn_{Bi} antisites [39].

We additionally find that T_{ex} consistently occurs between 230 and 260 meV in four samples (see Table I and [34]) that have vastly different carrier densities. This is an unexpected finding since the Fermi energy E_f must cross the conduction or valence band in $MnBi_2Te_4$, which yields a Moss-Burstein shift of T_{ex} to higher energies by an amount proportional to E_f for each specific sample. Since T_{ex} does not follow this expectation, we conclude that it cannot be a transition at a small momentum off the Γ point. This can imply that the magnetic exchange splitting at the Γ point is giant and much larger than the differences in E_f between different samples or that T_{ex} is a transition

TABLE I. Carrier density, thickness, and transition energy of the four samples studied here. The carrier density is extracted from Hall measurements at 5 K or below (see Supplemental Fig. 1) [34]. The transition energy is extracted from Fig. 1 for ND and JKU and from the data in [34] for ND-2 and ND-3. The uncertainty is determined by fitting the minimum observed in relative transmission. For sample ND, the uncertainty is the standard deviation taken on the two measurements shown in Fig. 3(d).

Sample ID	Carrier density	Thickness, substrate	Transition energy (T_{ex}) at 5 T
ND	$n = 2.2 \times 10^{19}$ cm^{-3}	41 nm/GaAs(111)	234 ± 2 meV
JKU	$p = 7.6 \times 10^{19}$ cm^{-3}	200 nm/SrF_2	257 ± 1 meV
JKU-2	$n = 2.3 \times 10^{19}$ cm^{-3}	200 nm/BaF_2	
ND-2	$n = 4.6 \times 10^{19}$ cm^{-3}	27 nm/GaAs(111)	237 ± 6 meV
ND-3	$p = 2.8 \times 10^{19}$ cm^{-3}	83 nm/GaAs(111)	255 ± 4 meV

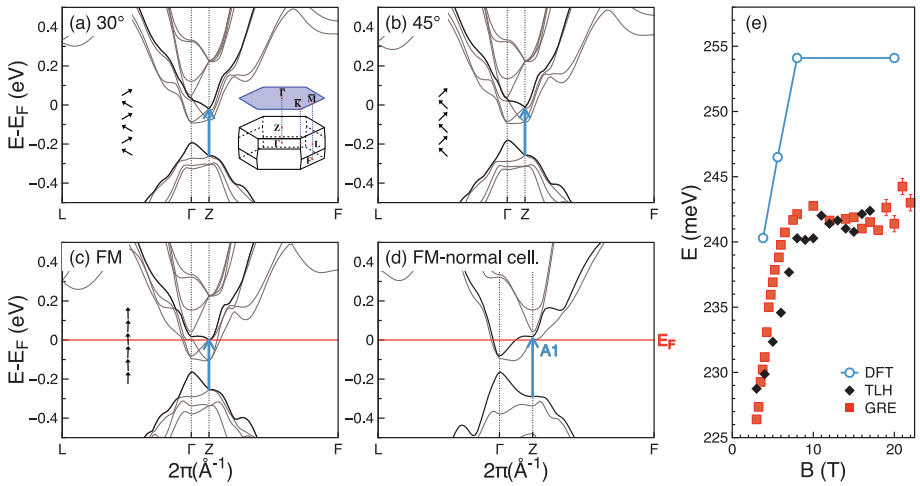

FIG. 4. Density functional theory (DFT) calculations compared with experimental data. Band structure of $MnBi_2Te_4$ with canting angles of (a) 30° and (b) 45° with respect to the horizontal. Band structure of FM $MnBi_2Te_4$ computed using a single (c) and double (d) unit-cell model [34]. E_f marks the Fermi energy determined by Hall effect measurements in [34]. A_1—the blue arrow—highlights the transition from valence band 1 (VB1) to conduction band 2 (CB2) at the Z point. The two bands of interest are bolded in (a)–(d). (e) Transition energy of A_1 (DFT) compared to the experimental data obtained in Grenoble (GRE) and Tallahassee (TLH) on sample ND. The magnetic field dependence of A_1 is obtained by converting the canting angle to magnetic field using Fig. 3(e).

occurring between other band extrema at a high symmetry point away from Γ.

While our data does not provide a definitive answer, density functional theory (DFT) calculations favor an interpretation involving an interband transition at the Z point of the Brillouin zone [see Fig 4(a)]. We compare our experimental results to DFT by computing the band structure for two canting angles (30° and 45°) and for the ferromagnetic state [blue dots in Fig. 3(e)]. The DFT scheme is based on the model from Ref. [20,40] (details in [34] and references therein [26,41–48]). The calculation of the band structure for these three magnetic states allows us to track the field dependence of T_{ex}, excluding the cyclotron and Zeeman effects. The results are shown in Figs. 4(a)–4(d) where the interband transition at the Z point is highlighted by the blue arrow and labeled A_1. Interband transitions involving the two lowest conduction bands at the Γ point are Pauli blocked because their edges fall below the Fermi energy [see Figs. 4(c) and 4(d)]. However, A_1 is not. The magnetization (and field) dependence of A_1 is extracted from Figs. 4(a)–4(c) and plotted in Fig. 4(e). It shows remarkable agreement with the experimental data, for model parameters taken from Ref. [44], despite a slight overestimation of the transition energies. The DFT model is also not consistent with T_{ex} occuring at the Γ point because it yields a magnetic exchange splitting that is too small compared to E_f to allow a transition energy independent from carrier density. DFT thus favors that a transition at the Z point is the cause of T_{ex} and the BC-induced MCD.

We have hence shown that an IR-MCD signal is activated by the onset of the canted magnetic state in $MnBi_2Te_4$ and scales in intensity with the nonquantized anomalous Hall conductivity, tying it to a topological phase transition that activates a BC. A comparison with first-principles calculations indicates that this MCD is likely due to an optical transition occurring at the Z point of $MnBi_2Te_4$ where the activated BC remains large. Our results demonstrate how resonant MCD can be used to track the changing Berry curvature through the evolving magnetic phase diagram of $MnBi_2Te_4$ films under a magnetic field despite native doping. Unlike the static Hall conductivity, resonant MCD is only sensitive to intrinsic band contributions to the dynamic Hall response, crucial to reliably extract BC. Our result motivates future studies of the resonant magneto-optical response of other magnetic materials expected to host a large BC, including other intrinsic magnetic TIs [49–52], extrinsic magnetic TIs [53], chiral magnets [54], and altermagnets [55]. Broadly speaking, we demonstrate that resonant MCD and magneto-optical absorption can be regarded as interesting complementary schemes to probe the quantum geometry tensor, since they directly probe the quantum mechanical transition dipole matrix element [12,56,57].

Acknowledgments—B. A. A., J. W., S. K. B., and X. L. acknowledge support from National Science Foundation Grant No. DMR-1905277. K. Y. acknowledges support from the Department of Energy Basic Energy Science Award No. DE-SC0024291. Y.-T. H. acknowledges support from National Science Foundation Grant No. DMR-2238748. A portion of this work was performed at the National High Magnetic Field Laboratory, which is supported by National Science Foundation Cooperative Agreements No. DMR-1644779, No. DMR-2128556,

and the State of Florida. G. S., S. W., A. N., and G. B. acknowledge support from the Austrian Science Funds Grant No. I-4493, AI0656811/21 and 10.55776/PIN6540324, as well as the JKU-Linz Grant No. LIT-2022-11-SEE-131. X. S. and B. P. are supported by ANR-20-CE30-0015-01. The authors acknowledge the support of the LNCMI-CNRS in Grenoble, a member of the European Magnetic Field Laboratory (EMFL).

The contributions of the authors supported by the Department of Energy and the National Science Foundation are as follows. B. A. A., J. W., S. K. B., and X. L. performed the material synthesis, structural characterization, and magnetotransport measurements of the anomalous Hall effect and magneto-optical measurements on the ND samples. K. Y. performed the high field magneto-optical measurements with circular polarization that revealed the MCD linked to Berry curvature. Y.-T. H. performed the analysis of the Hall conductivity sum rule.

[1] P. J. Stephens, Magnetic circular dichroism, Annu. Rev. Phys. Chem. **25**, 201 (1974).
[2] M. Berciu *et al.*, Origin of magnetic circular dichroism in GaMnAs: Giant Zeeman splitting versus spin dependent density of states, Phys. Rev. Lett. **102**, 247202 (2009).
[3] M. Dobrowolska, K. Tivakornsasithorn, X. Liu, J. K. Furdyna, M. Berciu, K. M. Yu, and W. Walukiewicz, Controlling the Curie temperature in (Ga, Mn)As through location of the Fermi level within the impurity band, Nat. Mater. **11**, 444 (2012).
[4] C. Autieri, C. Śliwa, R. Islam, G. Cuono, and T. Dietl, Momentum-resolved spin splitting in Mn-doped trivial CdTe and topological HgTe semiconductors, Phys. Rev. B **103**, 115209 (2021).
[5] L. Asteria, D. T. Tran, T. Ozawa, M. Tarnowski, B. S. Rem, N. Fläschner, K. Sengstock, N. Goldman, and C. Weitenberg, Measuring quantized circular dichroism in ultracold topological matter, Nat. Phys. **15**, 449(R) (2019).
[6] D. T. Tran, N. R. Cooper, and N. Goldman, Quantized Rabi oscillations and circular dichroism in quantum Hall systems, Phys. Rev. A **97**, 061602 (2018).
[7] M. Schüler and P. Werner, Tracing the nonequilibrium topological state of Chern insulators, Phys. Rev. B **96**, 155122 (2017).
[8] D. T. Tran, A. Dauphin, A. G. Grushin, P. Zoller, and N. Goldman, Probing topology by "heating": Quantized circular dichroism in ultracold atoms, Sci. Adv. **3**, e1701207 (2017).
[9] C. Lei and A. H. MacDonald, Kerr, Faraday, and magneto-electric effects in $MnBi_2Te_4$ thin films, Phys. Rev. B **108**, 125424 (2023).
[10] B. Ghosh, Y. Onishi, S.-Y. Xu, H. Lin, L. Fu, and A. Bansil, Probing quantum geometry through optical conductivity and magnetic circular dichroism, arXiv:2401.09689.
[11] Q. Ma, A. G. Grushin, and K. S. Burch, Topology and geometry under the nonlinear electromagnetic spotlight, Nat. Mater. **20**, 1601 (2021).
[12] J. Ahn, G.-Y. Guo, N. Nagaosa, and A. Vishwanath, Riemannian geometry of resonant optical responses, Nat. Phys. **18**, 290 (2022).
[13] P. Törmä, Essay: Where can quantum geometry lead us?, Phys. Rev. Lett. **131**, 240001 (2023).
[14] I. Souza and D. Vanderbilt, Dichroic f-sum rule and the orbital magnetization of crystals, Phys. Rev. B **77**, 054438 (2008).
[15] M. Schüler, U. De Giovannini, H. Hübener, A. Rubio, M. A. Sentef, and P. Werner, Local Berry curvature signatures in dichroic angle-resolved photoelectron spectroscopy from two-dimensional materials, Sci. Adv. **6**, eaay2730 (2020).
[16] I. Komissarov, T. Holder, and R. Queiroz, The quantum geometric origin of capacitance in insulators., Nat. Commun. **15**, 4621 (2024).
[17] B. Xu *et al.*, Infrared study of the multiband low-energy excitations of the topological antiferromagnet $MnBi_2Te_4$, Phys. Rev. B **103**, L121103 (2021).
[18] J. Ahn, S. Y. Xu, and A. Vishwanath, Theory of optical axion electrodynamics and application to the Kerr effect in topological antiferromagnets, Nat. Commun. **13**, 7615 (2022).
[19] C. Lei, O. Heinonen, A. H. MacDonald, and R. J. McQueeney, Metamagnetism of few-layer topological antiferromagnets, Phys. Rev. Mater. **5**, 064201 (2021).
[20] M. M. Otrokov *et al.*, Prediction and observation of an antiferromagnetic topological insulator, Nature (London) **576**, 416 (2019).
[21] K. He, $MnBi_2Te_4$-family intrinsic magnetic topological materials, npj Quantum Mater. **5**, 2 (2020).
[22] E. D. L. Rienks *et al.*, Large magnetic gap at the Dirac point in $Bi_2Te_3/MnBi_2Te_4$ heterostructures, Nature (London) **576**, 423 (2019).
[23] J.-Q. Yan, Q. Zhang, T. Heitmann, Z. Huang, K. Y. Chen, J.-G. Cheng, W. Wu, D. Vaknin, B. C. Sales, and R. J. McQueeney, Crystal growth and magnetic structure of $MnBi_2Te_4$, Phys. Rev. Mater. **3**, 064202 (2019).
[24] C. Liu, Y. Wang, H. Li, Y. Wu, Y. Li, J. Li, K. He, Y. Xu, J. Zhang, and Y. Wang, Robust axion insulator and Chern insulator phases in a two-dimensional antiferromagnetic topological insulator, Nat. Mater. **19**, 522 (2020).
[25] J. Li, Y. Li, S. Du, Z. Wang, B.-L. Gu, S.-C. Zhang, K. He, W. Duan, and Y. Xu, Intrinsic magnetic topological insulators in van der Waals layered $MnBi_2Te_4$-family materials, Sci. Adv. **5**, eaaw5685 (2019).
[26] S.-K. Bac *et al.*, Topological response of the anomalous Hall effect in $MnBi_2Te_4$ due to magnetic canting, npj Quantum Mater. **7**, 46 (2022).
[27] P. M. Sass, J. Kim, D. Vanderbilt, J. Yan, and W. Wu, Robust A-type order and spin-flop transition on the surface of the antiferromagnetic topological insulator $MnBi_2Te_4$, Phys. Rev. Lett. **125**, 037201 (2020).
[28] J.-Q. Yan, Q. Zhang, T. Heitmann, Z. Huang, K. Y. Chen, J.-G. Cheng, W. Wu, D. Vaknin, B. C. Sales, and R. J. McQueeney, Crystal growth and magnetic structure of $MnBi_2Te_4$, Phys. Rev. Mater. **3**, 064202 (2019).
[29] A. Zeugner *et al.*, Chemical aspects of the candidate antiferromagnetic topological insulator $MnBi_2Te_4$, Chem. Mater. **31**, 2795 (2019).

[30] Y. Bai *et al.*, Quantized anomalous Hall resistivity achieved in molecular beam epitaxy-grown $MnBi_2Te_4$ thin films, Natl. Sci. Rev. **11**, nwad189 (2024).
[31] S. K. Chong, C. Lei, S. H. Lee, J. Jaroszynski, Z. Mao, A. H. MacDonald, and K. L. Wang, Anomalous Landau quantization in intrinsic magnetic topological insulators, Nat. Commun. **14**, 4805 (2023).
[32] Z. Lian *et al.*, Antiferromagnetic quantum anomalous Hall effect modulated by spin flips and flops, arXiv:2405.08686.
[33] L. Tai *et al.*, Distinguishing the two-component anomalous Hall effect from the topological Hall effect, ACS Nano **16**, 17336 (2022).
[34] See Supplemental Material at http://link.aps.org/supplemental/10.1103/PhysRevLett.134.016601 for details on growth, the magnetooptical setups, additional magnetotransport measurements, additional characterization, the derivation of the sum rule, magnetooptical measurements of samples ND-2 and ND-3, and details of the DFT model.
[35] Y. Onishi and L. Fu, Fundamental bound on topological gap, Phys. Rev. X **14**, 011052 (2024).
[36] D. Xiao, M. C. Chang, and Q. Niu, Berry phase effects on electronic properties, Rev. Mod. Phys. **82**, 1959 (2010).
[37] D. Xiao, J. Shi, and Q. Niu, Berry phase correction to electron density of states in solids, Phys. Rev. Lett. **95**, 137204 (2005).
[38] D. L. Mills, Surface spin-flop state in a simple antiferromagnet, Phys. Rev. Lett. **20**, 18 (1968).
[39] Y. Lai, L. Ke, J. Yan, R. D. McDonald, and R. J. McQueeney, Defect-driven ferrimagnetism and hidden magnetization in $MnBi_2Te_4$, Phys. Rev. B **103**, 184429 (2021).
[40] M. M. Otrokov, I. P. Rusinov, M. Blanco-Rey, M. Hoffmann, A. Y. Vyazovskaya, S. V. Eremeev, A. Ernst, P. M. Echenique, A. Arnau, and E. V. Chulkov, Unique thickness-dependent properties of the van der Waals interlayer antiferromagnet $MnBi_2Te_4$ films, Phys. Rev. Lett. **122**, 107202 (2019).
[41] G. Kresse and J. Furthmüller, Efficient iterative schemes for *ab initio* total-energy calculations using a plane-wave basis set, Phys. Rev. B **54**, 11169 (1996).
[42] G. Kresse and D. Joubert, From ultrasoft pseudopotentials to the projector augmented-wave method, Phys. Rev. B **59**, 1758 (1999).
[43] G. Kresse and J. Furthmüller, Efficiency of ab-initio total energy calculations for metals and semiconductors using a plane-wave basis set, Comput. Mater. Sci. **6**, 15 (1996).
[44] M. M. Otrokov, T. V. Menshchikova, I. P. Rusinov, M. G. Vergniory, V. M. Kuznetsov, and E. V. Chulkov, Magnetic extension as an efficient method for realizing the quantum anomalous Hall state in topological insulators, JETP Lett. **105**, 297 (2017).
[45] P. E. Blöchl, Projector augmented-wave method, Phys. Rev. B **50**, 17953 (1994).
[46] J. P. Perdew, K. Burke, and M. Ernzerhof, Generalized gradient approximation made simple, Phys. Rev. Lett. **77**, 3865 (1996).
[47] S. Grimme, J. Antony, S. Ehrlich, and H. Krieg, A consistent and accurate *ab initio* parametrization of density functional dispersion correction (DFT-D) for the 94 elements H-Pu, J. Chem. Phys. **132** (2010).
[48] D. S. Lee, T. H. Kim, C. H. Park, C. Y. Chung, Y. S. Lim, W. S. Seo, and H. H. Park, Crystal structure, properties and nanostructuring of a new layered chalcogenide semiconductor, Bi_2MnTe_4, CrystEngComm **15**, 5532 (2013).
[49] S. X. M. Riberolles *et al.*, Magnetic crystalline-symmetry-protected axion electrodynamics and field-tunable unpinned Dirac cones in $EuIn_2As_2$, Nat. Commun. **12**, 999 (2021).
[50] Y. Xu, Z. Song, Z. Wang, H. Weng, and X. Dai, Higher-order topology of the axion insulator $EuIn_2As_2$, Phys. Rev. Lett. **122**, 256402 (2019).
[51] M. Abdul Karim, J. Wang, D. Graf, K. Yoshimura, S. Bey, T. Orlova, M. Zhukovskyi, X. Liu, and B. A. Assaf, Molecular beam epitaxy growth of axion insulator candidate $EuIn_2As_2$, Phys. Rev. Mater. **7**, 104202 (2023).
[52] I. Levy, C. Forrester, H. Deng, M. Roldan-Gutierrez, M. R. McCartney, D. J. Smith, C. Testelin, L. Krusin-Elbaum, and M. C. Tamargo, Compositional control and optimization of molecular beam epitaxial growth of $(Sb_2Te_3)_{1-x}(MnSb_2Te_4)_x$ magnetic topological insulators, Cryst. Growth Des. **22**, 3007 (2022).
[53] C.-Z. Chang *et al.*, Experimental observation of the quantum anomalous Hall effect in a magnetic topological insulator, Science **340**, 167 (2013).
[54] X. Li, J. Koo, Z. Zhu, K. Behnia, and B. Yan, Field-linear anomalous Hall effect and Berry curvature induced by spin chirality in the kagome antiferromagnet Mn_3Sn, Nat. Commun. **14**, 1642 (2023).
[55] L. Šmejkal, J. Sinova, and T. Jungwirth, Beyond conventional ferromagnetism and antiferromagnetism: A phase with nonrelativistic spin and crystal rotation symmetry, Phys. Rev. X **12**, 031042 (2022).
[56] N. Wang *et al.*, Quantum-metric-induced nonlinear transport in a topological antiferromagnet, Nature (London) **621**, 487 (2023).
[57] A. Gao *et al.*, Quantum metric nonlinear Hall effect in a topological antiferromagnetic heterostructure, Science **381**, 181 (2023).

Correction: A minor error in a support statement in the Acknowledgments section has been fixed and author contribution information has been added.